



Regular article

Noninvasive blood glucose sensing by near-infrared spectroscopy based on PLSR combines SAE deep neural network approach

Guang Han^{a,b,c}, Siqi Chen^a, Xiaoyan Wang^a, Jinhai Wang^a, Huiquan Wang^a, Zhe Zhao^{a,*}^a Department of Life Sciences, Tiangong University, Tianjin 300387, China^b Department of Precision Instrument and Optoelectronics Engineering, Tianjin University, Tianjin 300072, China^c Tianjin Shareshine Technology Co, LTD, Tianjin 300384, China

ARTICLE INFO

ABSTRACT

Keywords:

Near-infrared spectroscopy
Noninvasive blood glucose predication
Partial least square regression
Stacked auto-encoder deep neural network
Clarke error grid analysis

Near-infrared spectroscopy has been considered as one of the most effective methods for noninvasive blood glucose sensing. Due to the strong scattering of human tissues and the differences among individuals, the relationship between spectral data and blood glucose concentration is nonlinear. Therefore, the linear prediction model has limitations when modeling multiple human samples. The present paper proposes a hybrid model in order to improve the prediction accuracy and versatility of the method, which was based on integrated linear partial least square regression (PLSR) with the nonlinear stacked auto-encoder (SAE) deep neural network. In this work, the diffuse reflectance spectrum of the palm was measured at six different wavelengths in 19 healthy subjects. The prediction results of multiple samples demonstrated that the correlation coefficients of the PLSR-SAE model is improved from 0.3021 to 0.9216 on average, which significantly optimizes the prediction effect compared with the traditional PLSR model. In addition, the prediction accuracy of Support Vector Regression (SVR) model and PLSR-SAE model are 0.8243 and 0.9216 respectively. Furthermore, in Clarke error grid analysis, the PLSR-SAE model could achieve 97.96% of points in A region, which has demonstrated that the prediction accuracy of this noninvasive blood glucose detection method might meets the precision range of clinical laboratory standards. Furthermore, it shows the potential of combining linear and nonlinear regression models for noninvasive prediction of other blood components.

1. Introduction

In the recent years, the number of people with diabetes has been increasing rapidly worldwide. According to the International Diabetes Federation Diabetes Atlas Ninth Edition [1], it is estimated that 463 million adults have diabetes in 2019, and this number is predicted to reach 578 million and 700 million by 2030 and 2045, respectively.

Most of the currently used blood glucose monitoring methods are invasive and require drawing blood by finger-prick or vein puncture [2]. The long-term effects of devices for monitoring blood glucose concentration levels can cause severe pain in some patients and may lead to tissue infection and vascular damage. Likewise, minimally-invasive techniques have been proposed, such as the measurement of interstitial fluid [3], reverse iontophoresis or microdialysis, which may only impose the skin tissue damage rather than damage of blood vessels [4]. Meanwhile, scientists are actively developing painless, safe, rapid and accurate noninvasive blood glucose detection methods [5].

Various noninvasive blood glucose measurement methods based on different technologies have been previously published in the literature, such as polarimetry [6], photoacoustic spectroscopy [7], bio-electrical impedance spectroscopy [8], thermal emission [9], optics and other technologies [10]. In particular, optical techniques are recognized as highly accurate, painless and safe noninvasive glucose measurement techniques [11], e.g. optical coherence tomography [12,13], microwave spectroscopy [14], near-infrared spectroscopy (NIRS) [15–18], mid-infrared spectroscopy (MIRS) [19], Raman spectroscopy [20,21] and visible laser light [22]. Among above-mentioned optical techniques, NIRS is considered as one of the most effective and rapid noninvasive technique due to the light in the near-infrared region allows much deeper penetration within the tissue than in the visible light region or MIRS region, determining the concentrations of glucose much better [18].

In order to improve the prediction accuracy robustness of NIRS, multiple measurement methods based on different absorption bands in

* Corresponding author.

E-mail addresses: hanguang@tju.edu.cn (G. Han), zhaozhe@tiangong.edu.cn (Z. Zhao).

electromagnetic spectrum and at different anatomical locations, such as finger, forearm, palm and tongue, have been studied in both clinical and home trials [12–16]. For example, Ping et al. (2005) conducted measurements of diffuse reflectance spectra at the palm, wrist and thumb tip [17]. This study demonstrated that the root mean square error of prediction (RMSEP) value of 0.835 mmol/L of individual sample of thumb tip [17].

Nevertheless, the glucose absorption spectra may overlap with other absorbing components in human biological tissues, e.g. water, hemoglobin and lipids [18,19], which then makes it difficult to analyze the glucose absorption information in NIR band region. Contrarily, chemometrics methods, such as Multivariate Linear Regression (MLR), Partial Least Square Regression (PLSR) and Principal Component Regression (PCR), are frequently used for extracting data from multivariate information in order to optimize the measurement process, and therefore these methods offer considerably easier extraction of glucose absorption information from the spectrum. According to the Beer-Lambert law of linear regression method, it is assumed that the light attenuation is linearly proportional to the blood glucose concentration and that analyzed samples are non-scattering. However, there is a nonlinear relationship between the glucose absorption spectrum and its concentration. Moreover, when using NIRS for quantitative analysis, there is 80% of the error attenuation as a result of scattering characteristics of the tissue [18]. Therefore, establishing a non-linear regression model, such as artificial neural network (ANN), non-linear autoregressive (NAR) neural network and long short-term memory (LSTM) network [23], may be more suitable for noninvasive blood glucose predication. Chuah and Raveendran et al. (2009) calibrated Individual data by using PLSR and back-propagation (BP) neural network [20]. It was reported that the approach based on BP model appreciably improves the prediction accuracy of results, in comparison to the linear PLSR model.

Deep neural network is an extension of a traditional ANN, providing a multi-level network model that mimics the human brain and eliminates the need for manual representation learning and analyzing, as required by ANN [24,25]. The stacked auto-encoder (SAE) deep neural network is a neural learning model composed of three layers: input, hidden and output layers. The SAE uses a training process of unsupervised learning features per each layer, which results in considerably improved prediction accuracy of the calibration model [26–28].

Taking into consideration that a deep neural network can eliminate or suppress the nonlinear spectral noise introduced in the correction model, this study introduces SAE deep neural network as a prediction model for noninvasive blood glucose detection in order to achieve significant improvement in the prediction accuracy of the present model. Here, the absorbance relationship between the blood components and incident light frequency has an important role in the calibration model. A suitable region for noninvasive glucose level monitoring with greater absorption of glucose than that of the other blood components appears to be at the wavelength regions greater than 1050 nm [29]. In order to verify the feasibility of using SAE deep neural network to detect blood glucose components, we first take intralipid solutions with different concentrations as the research objects, modeling and predicting the glucose concentration under multiple spectra. The results show that SAE neural network has high applicability to the prediction of turbid medium concentration [30].

The glucose absorption signatures might appear at the wavelengths near 1150 nm and 1600 nm in the near infrared band of 1000–1700 nm. In this study, we measured the diffuse reflectance spectrum of 19 non-diabetic subjects' palms at six different wavelengths in the range of 1050–1609 nm. A contact measurement system connected to a palm and fiber optic probes was used to collect spectral data. The oral glucose tolerance test experiments (OGTTs) were performed in each subject. First, we used the PLSR model and the SAE model to model the overall sample respectively. The present experimental findings demonstrated that PLSR model has better prediction capabilities than SAE model when

modeling a single sample. However, for multiple samples, the prediction effect of the PLSR model is significantly worse than that of the SAE model.

Accordingly, this paper proposes a noninvasive blood glucose predication method based on integrated PLSR model with SAE deep neural network. First, the collected data were calibrated by PLSR model. Further, the samples with poor correlation were eliminated from the PLSR model by using SAE, which enabled a straightforward extraction of features from layer to layer between multiple-hidden layers of the present network model to improve a prediction accuracy of the final outcomes. It has been demonstrated here that the prediction effect of SAE model is better than that of the PLSR and SVR models, and the PLSR-SAE model facilitates better prediction accuracy effect in comparison to the SAE model when modeling multiple samples. In the present work, it has been demonstrated that the prediction accuracy of the noninvasive blood glucose predication method based on integrated PLSR model with SAE deep neural network meets the precision range of clinical laboratory standards, which has certain potential in clinical research and trials.

2. Theory and PLSR-SAE algorithm

2.1. Stacked Auto-encoder (SAE) deep neural network

SAE deep neural network is an unsupervised learning network model composed of multiple layers of sparse auto-encoders (AE) [26]. The output of the former AE is used as an input of the latter model. When there is a n-layer SAE network, it can be assumed that $W_1^{(i)}, W_2^{(i)}, b_1^{(i)}, b_2^{(i)}$ represent the weight and bias and that they correspond to the AE at the layer i . In addition, AE is composed of encoder and decoder, and the SAE neural network can be mainly divided into two separate processes [27]:

1. Training process

It is represented using the encoding phase in which information is transmitted from front to back:

$$h^{(i)} = f(z^{(i)}) \quad (1)$$

$$z^{(i+1)} = W_1^{(i)} h^{(i)} + b_1^{(i)} \quad (2)$$

2. Fine-tuning process

It is represented by the decoding phase of information transmission from back to front:

$$h^{(n+i)} = f(z^{(n+i)}) \quad (3)$$

$$z^{(n+i+1)} = W_2^{(n-i)} h^{(n+i)} + b_2^{(n-i)} \quad (4)$$

There are typically three layers within the sparse AE: input, hidden and output layers. Among them, $h^{(i)}$ is the output of the AE at the layer i , $h^{(n)}$ is the output of the final hidden layer, which can be further defined as a feature of the Softmax classifier. f represents the activation function, which is used by both the hidden and output layers [31].

In the present work the nonlinear Sigmoid function was conducted as follows:

$$f(x) = \frac{1}{1 + e^{-x}} \quad (5)$$

The SAE deep neural network adopts greedy layer-wise unsupervised pre-training method, and the whole network is fine-tuned by back-propagation, as shown in Fig. 1. The fine-tuning process optimizes the weight and bias $\{W_j, b_j\}$ ($j = 1, 2, \dots, L$) by minimizing the prediction error of the labeled variables. The back-propagation function as follows:

- Training Process: Layer-wise unsupervised pre-training



- Fine-tuning Process: Supervised fine-tuning

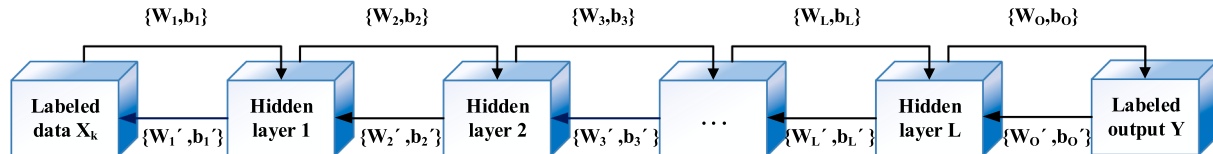


Fig. 1. The training and fine-tuning process of SAE deep neural network.

$$B_O = \sum_{k=1}^N \left\| y_k - \hat{y}_k \right\|^2 / 2N \quad (6)$$

where N is the total number of training samples, y_k and \hat{y}_k represent the labeled value and predicted value of the data sample k , respectively.

Then, we take classification as an example to describe the training process, the input data of training is $X = \{X_1, X_2, \dots, X_N\}, N = 6$.

The original input X_k is utilized as an input in the training process of the first auto-coding neural network, with its corresponding weight and bias ($W_1^{(1)}, W_2^{(1)}, b_1^{(1)}, b_2^{(1)}$), as shown in Fig. 2. The output of the first hidden layer $h_k^{(1)}$ is called the first-order feature, which represents the input of the second auto-encoder. The aforementioned output of the present hidden layer will continue to train the second auto-coding neural network in order to obtain the adequate weight and bias ($W_1^{(2)}, W_2^{(2)}, b_1^{(2)}, b_2^{(2)}$). Likewise, the output of the second hidden layer $h_k^{(2)}$ can be obtained as the second-order feature. In succession, the parameters of SAE neural network can be trained layer-by-layer, where the second-order feature can be trained as an input of the Softmax classifier in

order to proceed with classification process.

The SAE deep neural network can automatically learn the hierarchical structure between obtained features through unsupervised automatic learning of the model represented layer-by-layer. During the entire process, the parameters of the previous layer remain unchanged while training the next layer. Every hidden layer can perform a nonlinear transformation of the output of the previous layer. With each additional hidden layer, the model can calculate a more complex state within the layers and obtain more accurate feature representation. Finally, after the initialization of the parameters, the network should proceed with the practice of fine-tuning of the global parameters. Proper tuning of the network weights and offset ensures lower error rates, making the SAE model more reliable by increasing its generalization.

2.2. PLSR-SAE algorithm

2.2.1. Correction and screening sample data by PLSR model

In this paper, Camo's Unscrambler software (The Unscrambler X) was used to proceed with PLSR analysis. PLSR is a multiple regression analysis technique, and thus, the input data set requires at least three

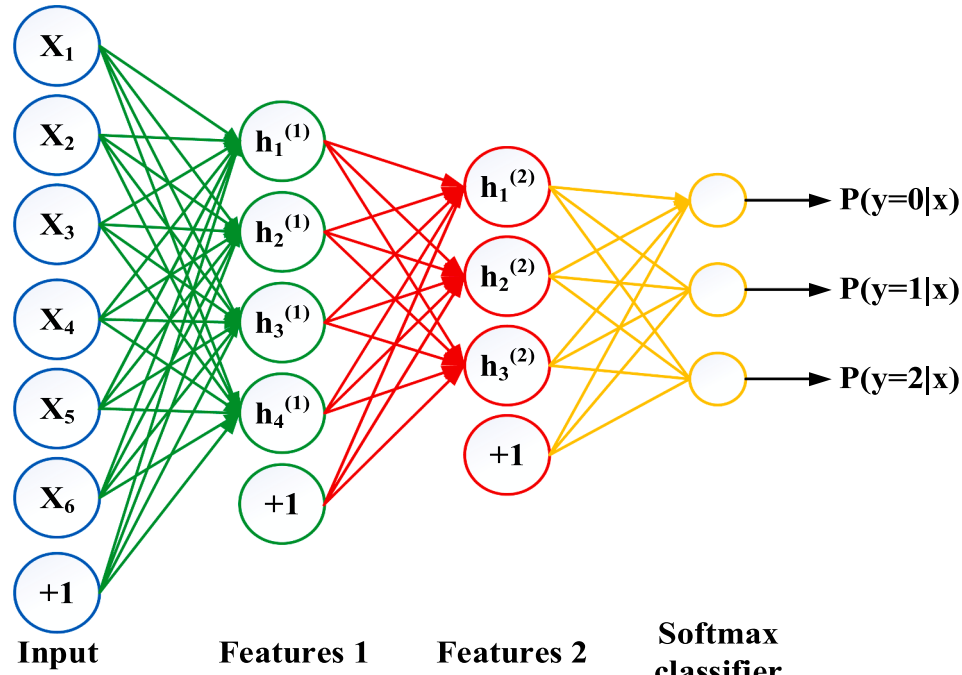


Fig. 2. The training process structure of SAE deep neural network.

samples (rows) and two variables (columns) to complete the calculation.

Firstly, the PLSR model was established for the 19 single samples data collected in the present experiment. For example, in Sample 7, the reference value of blood glucose concentration with the corresponding light intensity values was measured 19 times at six different wavelengths during the experiment. Therefore, the prediction matrix X was set to 19 sample points (rows) and seven input variables (columns), including blood glucose reference values for six different wavelengths. The response matrix Y selected the same 19 sample points (rows) and an output variable (column) as predicted values of blood glucose levels, which then ensures that the dimensions of the row set would match the one of the prediction matrix X. Further, a weighted standard deviation was applied to each variable of X and Y, and was represented as:

$$A/(SDev + B) \quad (7)$$

with the default A and B defined as 1 and 0, respectively.

In this paper, the model of PLSR algorithm was set as Kernel PLS, which is a single response variable and therefore there was none iteration. Finally, the leave-one-out cross validation was applied to the final PLSR modeling outcome, with the chosen optimal quantity for the uncertainty test.

Furthermore, the root mean square error of prediction (RMSEP), a correlation coefficient of prediction (R_p) and the Clarke Error Grid Analysis (EGA) were used as main indexes to evaluate the reliability and prediction ability of the calibration model [21]:

$$RMSEP = \sqrt{\frac{\sum_{i=1}^n (\hat{y}_i - y_i)^2}{n}} \quad (8)$$

$$R_p = \sqrt{\frac{\sum_{i=1}^n (\hat{y}_i - y_i)^2}{\sum_{i=1}^n (\bar{y}_i - y_i)^2}} \quad (9)$$

where n is the sample capacity, y_i and \hat{y}_i are the measured reference value and predicted value of blood glucose concentration, respectively. \bar{y}_i is the average value of the predicted blood glucose concentration level. Where R_p goes to '1', RMSEP value decreases, indicating improved predictive ability of the model.

A PLSR correction model with 19 individual samples has been established, where RMSEP and R_p were compared. Among the individual samples set, eight samples that met a following condition were excluded: $RMSEP > 0.6 \text{ mmol/L}$ or $R_p < 0.7$, and therefore the present model remained with the 11 chosen samples within the set. Accordingly, an overall sample included 219 sets of spectral data were set as input data sets of the SAE deep neural network. In addition, the overall sample set was also used in the individual PLSR correction model, and the results were further compared to the integrated PLSR-SAE model.

2.2.2. Modeling of SAE deep neural network

Here, a dual hidden layer SAE deep neural network was used to model the screened spectral data of PLSR model, with a four-layer network structure.

The input layer of SAE model was composed of six input neurons, that is, six wavelengths (1050 nm, 1219 nm, 1314 nm, 1409 nm, 1550 nm and 1609 nm), as shown in Fig. 3. Also, set of 219 groups of spectral data were used as input data sets, corresponding to 11 samples with a good correlation coefficient, after being screened by the PLSR model. The output layer had only one neuron, which was equal to the predicted value of blood glucose concentration level. According to the structure of the network, the number of hidden layers can be approximately calculated by:

$$H_1^2 = H_2 * \text{input} \quad (10)$$

$$H_2^2 = H_1 * \text{output} \quad (11)$$

Since there were six input variables and one output variable, we defined the first hidden layer H_1 to have four neurons and the second hidden layer H_2 to have two neurons.

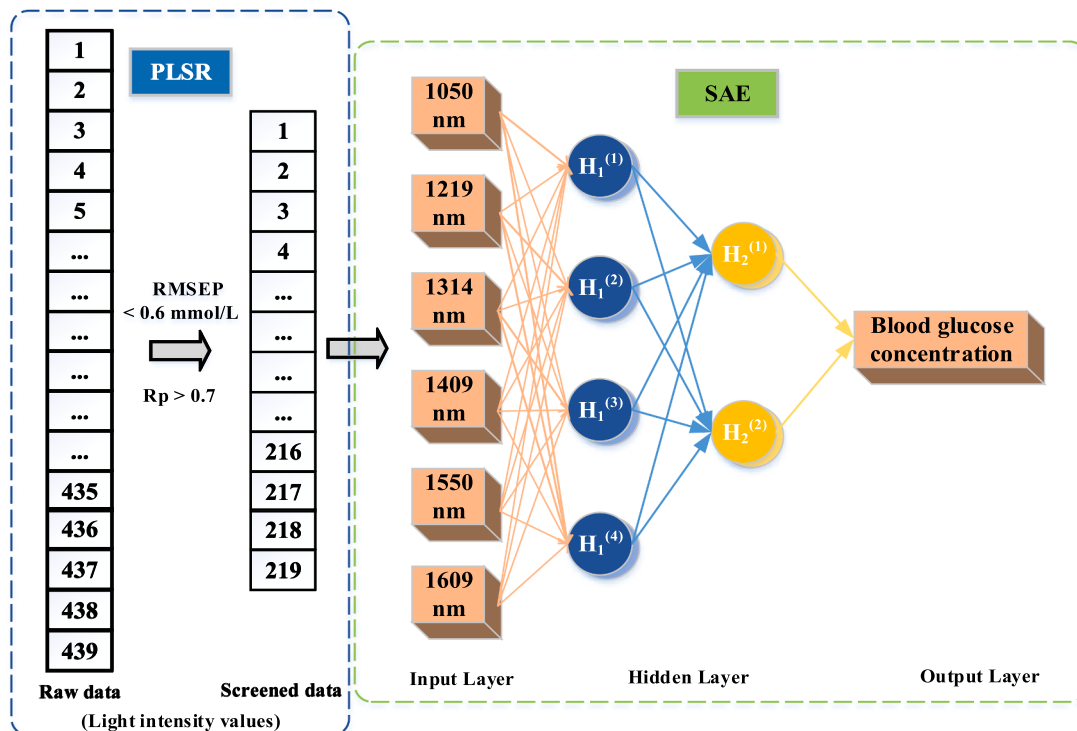


Fig. 3. Dual hidden layer structure of SAE deep neural network in PLSR-SAE model.

During the training phase of SAE neural network, we continually modeled the data set and adjusted the size of the training parameters to determine the most adequate parameter range with the significantly improved prediction effect. When the training epochs were within the range of 100–2000, the prediction effect was compared to different iteration times.

As demonstrated in Table 1 and Fig. 4, whenever the number of iterations increases, the stability of a correlation coefficient of prediction increases and the average RMSEP decreases accordingly. Additionally, the range of training epochs was different for the corresponding peak of different iteration times. The correlation coefficient of prediction was within the range between 0.77 and 0.92 when the iteration value equal to 1000. Also, its fluctuation range was lower than that of the other iteration. The two peaks corresponded to the training epochs at 400 and 1400.

Considering the over-fitting problem of deep neural network, the SAE model is optimized because the PLSR model screening process reduces the input data of neural network. Early stopping method is used to improve the generalization of the model. The accuracy of validation data is calculated at the end of each training epoch. When the accuracy meets the “no-improvement-in-30epochs” strategy, the training is stopped. Early stopping training can avoid the over fitting of SAE model to training data to a certain extent.

Therefore, the parameters of layer-by-layer training were defined as training epochs and iterations at 400 and 1000 at the first peak. Further, the unsupervised learning rate was 0.1, whereas the batch-size was 10. In this study, the training set was selected by using the random distribution. The input data were randomly sorted, the first 80% of data were selected as part of the training set and the remaining 20% were defined as the prediction set. Accordingly, from the 219 sample points, which were randomly sorted, the first 170 sample points were selected as the training set, and the last 49 sample points were defined as the prediction set to verify and predict the training results. As such, the loss function with the best iteration could have been selected per each prediction process in order to obtain the best prediction result.

3. Materials and methods

3.1. The experimental materials

As shown in Fig. 5, the experimental hardware system consisted of a light source, an optical switch (FSW1 × 1-SM-NL, CLP 34, China), an optical fiber bundle and an optical fiber probe (a quartz fiber with a core diameter of 0.28 mm), a detector and thermostat, a portable blood glucose meter (GT-1820, Arkray, Japan), data acquisition card (USB-6210 acquisition card, NI, USA) and computer.

The light source is an array composed of six Super Luminescent Emitting Diodes (SLD, InPhenix, USA), with the central wavelengths at 1050 nm, 1219 nm, 1314 nm, 1409 nm, 1550 nm and 1609 nm. The wattage of SLD at six wavelengths is different, which is about 5–10 mW. The near-infrared indium gallium arsenic detector (G12181-210 K, HAMAMATSU, Japan) is able to detect the spectral signal within the spectral range between 900 nm and 1850 nm.

In the present experimental work, a contact measurement system connected to a palm and fiber optic probes was used to collect spectral data. The measurement system had an integrated device, which could adjust the elastic pressure to avoid the influence of the contact pressure on tissue optical parameters and the large measurement errors. The

human-computer interface device is shown in Fig. 6.

In addition, the present findings showed that temperature changes of 0.1 °C may lead to the change in blood glucose concentration by 50 mg/dL. Also, it was shown that the errors, which were introduced by the temperature change, exceed the allowable errors in glucose measurements. Therefore, according to the individual temperature at the palm in each subject, the human-computer interface device should be able to control the stable body temperature within the range of 34–35.5 °C. We set the thermostat to 35 °C with the error of 0.1 °C.

3.2. Subjects and the experimental scheme

19 healthy volunteers (8 females and 11 males), aged 24–30 years (values are shown as mean 27 ± 3 standard deviation), were recruited for this study and provided informed consent. The subjects were not diabetic, obese or underweight according to the World Health Organization criteria.

The measurements were conducted at six different wavelengths (1050 nm, 1219 nm, 1314 nm, 1409 nm, 1550 nm and 1609 nm) and were controlled by the optical switch. One measurement session was taken at each wavelength frequency for 3 s, and was continuously recorded for approximately 20 s.

For this purpose, we conducted 19 experiments (some volunteers with 2 times) and obtained 19 data samples. The measurements were taken at the palm of the right hand of the subject, which was placed on the platform of the human-computer interface. The measurement site was recorded for approximately 10 min after the initial hand-interface contact in order to eliminate the errors introduced by external factors, such as temperature and measurement position. The measurement time in each subject was up to 2 h, depending on time when the blood glucose level would return to the fasting state in each subject. Also, the background signal was measured in the fasting state separately per each subject.

3.3. The experimental protocol

Specifically, we conducted OGTTs in order to obtain large changes in blood glucose concentration in the study group within 2 h. OGTT measures your body's response to glucose, which is currently recognized as a standard test to diagnose diabetes type-2, and it is widely employed in a clinical setting.

At the beginning of the OGTTs, subjects were given to drink an oral glucose solution with 75 g of glucose in 250 ml of water solution (with a peak value between 8.9 and 12.6 mmol/L) after fasting process of 8–14 h (approximately between 3.8 and 5.5 mmol/L). We used the vein detained needle to collect blood samples every 3–5 min in order to reduce discomfort of frequent needling. The standard value of blood glucose was measured by using a portable blood glucose meter. Furthermore, the average value was recorded and set as the basal, reference value, where the spectrum signals were collected simultaneously. A total of 12–36 sets of reference values and spectral signals were collected during the entire experimental process, depending on time of each subject's blood glucose returned to the fasting state.

4. Results

4.1. Prediction results of PLSR and SAE models

4.1.1. PLSR model with a single sample

In this study, we used Camo's Unscrambler software to evaluate the PLSR modeling and its analysis. Firstly, PLSR modeling was performed on a total of 19 spectral samples, with following the leave-one-out-cross validation (see Table 2). The gray grid in the Table 2 shows that eight samples resulted in $\text{RMSEP} > 0.6 \text{ mmol/L}$ or a correlation coefficient of prediction (R_p) < 0.7 , which were then excluded. The average predicted results (RMSEP and a correlation coefficient of prediction) were 0.7212

Table 1
Average prediction results of PLSR-SAE models at different iterations.

Iteration	RMSEP (mmol/L)	R _p
200	1.8128	0.6679
500	1.5283	0.7104
1000	1.2064	0.8287

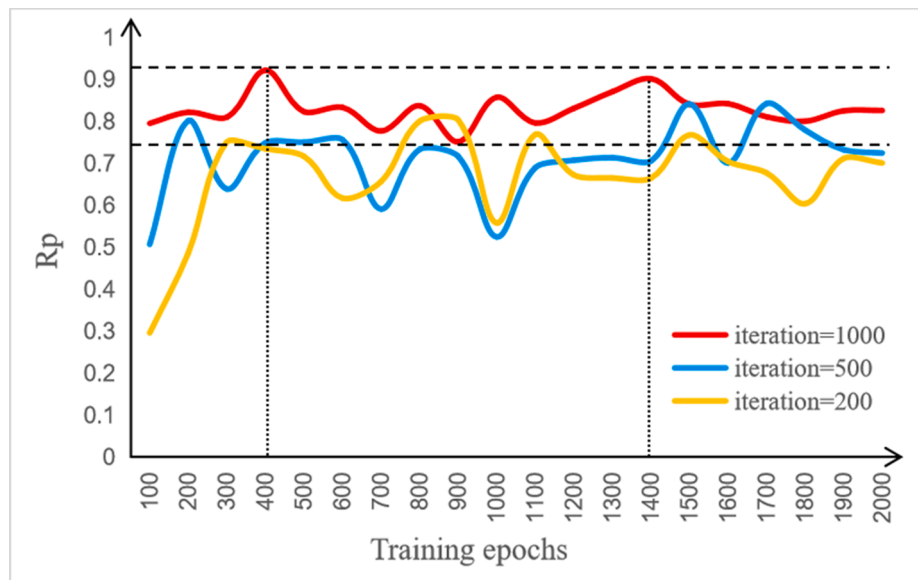


Fig. 4. The relation between the training epochs and correlation coefficient of prediction at different iterations.

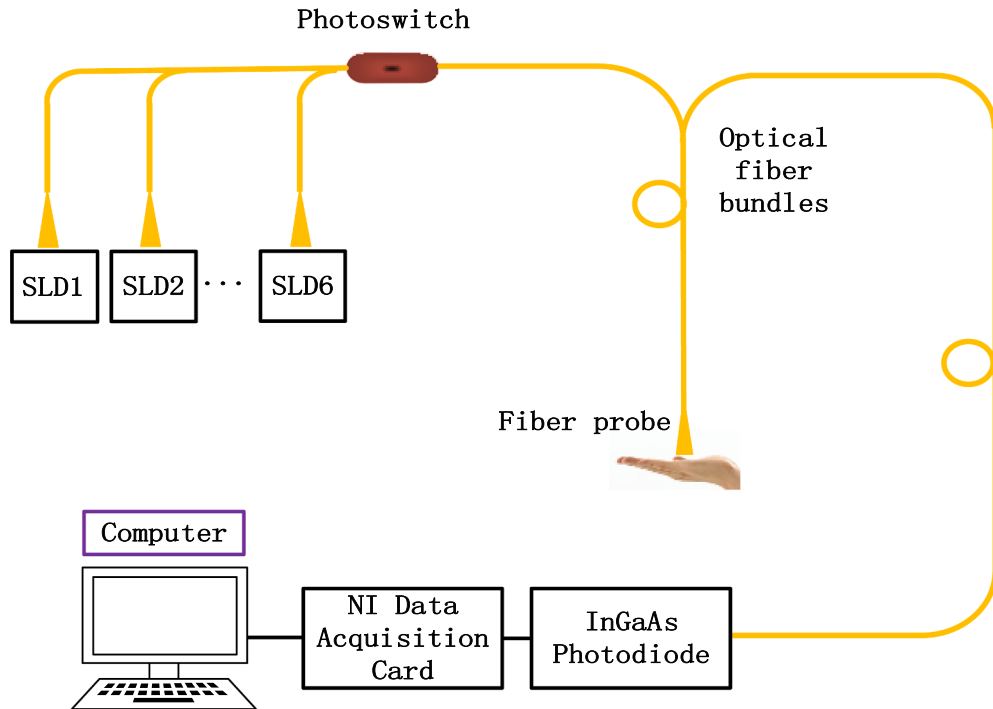


Fig. 5. The composition of the hardware system.

mmol/L and 0.7027, respectively, in PLSR model with 19 individual samples.

Among them, Sample 7 had the best prediction effect, as shown in Fig. 7. The error between the two corresponding values was negligible. The RMSEP was equal to 0.3632 mmol/L with a correlation coefficient of prediction of 0.9658, which is close to 1. Therefore, these results indicate that the PLSR model has a good prediction effect in a single sample.

4.1.2. PLSR model with multiple samples

Further, we integrated 19 samples into a set, which was defined as overall sample 1 (OS 1), with a total of 439 sample points. After using PLSR model to exclude eight samples with poor prediction effect, the

remaining 11 samples were further integrated into a set, which was recorded as overall sample 2 (OS 2). There were 219 sample points in total. Similarly, we used PLSR to model two sets of samples separately. Specifically, we compared the prediction results between these two sets, as well as to the average prediction value of a single sample model, as shown in Table 3.

It is demonstrated that the screening process of PLSR model reduces 220 samples with poor correlation by comparing these two sets of multiple samples. The PLSR model with OS 2 resulted in a lower RMSEP and greater correlation coefficient of prediction when compared to the corresponding values in OS 1. Moreover, compared to the average prediction results of PLSR model with a single sample, PLSR model has worse prediction effect for multiple samples.

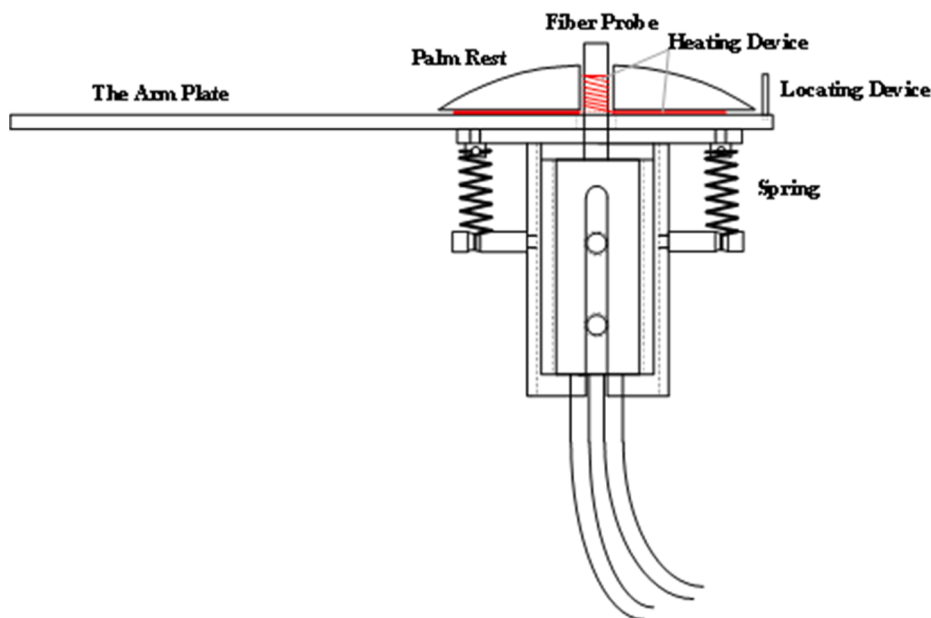


Fig. 6. The human-computer interface of the contact measurement system.

Table 2

Prediction results of PLSR model in each samples.

Samples	RMSEP	R _p	Samples	RMSEP	R _p
Sample 1	0.4075	0.7967	Sample 11	1.0319	0.7350
Sample 2	1.3810	0.1773	Sample 12	0.5535	0.8107
Sample 3	1.9906	0.2689	Sample 13	0.4202	0.9427
Sample 4	1.1507	0.6917	Sample 14	0.4041	0.8815
Sample 5	0.5315	0.8688	Sample 15	0.8211	0.4072
Sample 6	0.5173	0.8716	Sample 16	0.4626	0.8227
Sample 7	0.3632	0.9658	Sample 17	0.5696	0.5256
Sample 8	0.8212	0.4455	Sample 18	0.4949	0.7348
Sample 9	0.3288	0.9092	Sample 19	0.5634	0.8171
Sample 10	0.8886	0.6780	Mean	0.7212	0.7027

Moreover, Clarke error grid analysis (EGA) was used to evaluate the clinical accuracy. It demonstrated the error grid analysis between the reference and measured values. As shown in Fig. 8(a) and (b), the proportion of sample points in region A is 60.36% and 67.58%, whereas the proportion in region B is 39.18% and 31.96% in OS 1 and OS 2, respectively. Hence, the present findings evaluate that employing a PLSR screening process before integrating multiple samples as an input set, may improve the prediction effect of PLSR model of multiple samples. However, the prediction accuracy has not been significantly improved.

4.1.3. SAE model with multiple samples

Furthermore, OS1 is used as the input set of SAE model, and the prediction effect is compared with that of PLSR model. The RMSEP is 1.6719 mmol/L and 1.3368 mmol/L with correlation coefficients (R_p) of 0.1670 and 0.8373, respectively for PLSR and PLSR-SAE models (see Table 3). In addition, the proportion of sample points in region A is 60.36% and 80.90%, whereas the proportion in region B is 39.18% and 19.10% in PLSR and PLSR-SAE models respectively, as shown in Fig. 8 (a) and (c). The results show that the fitting and prediction capabilities

in SAE model are significant superior in comparison to PLSR model.

4.2. Comparison between PLSR, SVR and PLSR-SAE models

We combined SAE deep neural network with PLSR to establish correction models in multiple sample sets, and further to optimize the prediction effect in SAE model. In order to compare the prediction effect of the PLSR-SAE model, we further used the Support Vector Regression (SVR) method to model multiple samples.

4.2.1. Comparison between PLSR and PLSR-SAE model

After the screening process of PLSR, the prediction value of the blood glucose concentration was set as an output in PLSR-SAE model. The optimal iteration loss function was 2.83×10^{-6} . Comparing the prediction results in PLSR and PLSR-SAE models, the RMSEP is 1.3929 mmol/L and 1.0151 mmol/L with correlation coefficients (R_p) of 0.3021 and 0.9216, respectively (see Table 3). We found that PLSR-SAE model facilitates lower RMSEP with a greatly improved correlation coefficient of prediction, in comparison to the PLSR model. As shown in Fig. 8(b) and (d), PLSR and PLSR-SAE models have 67.58% and 97.96% sample

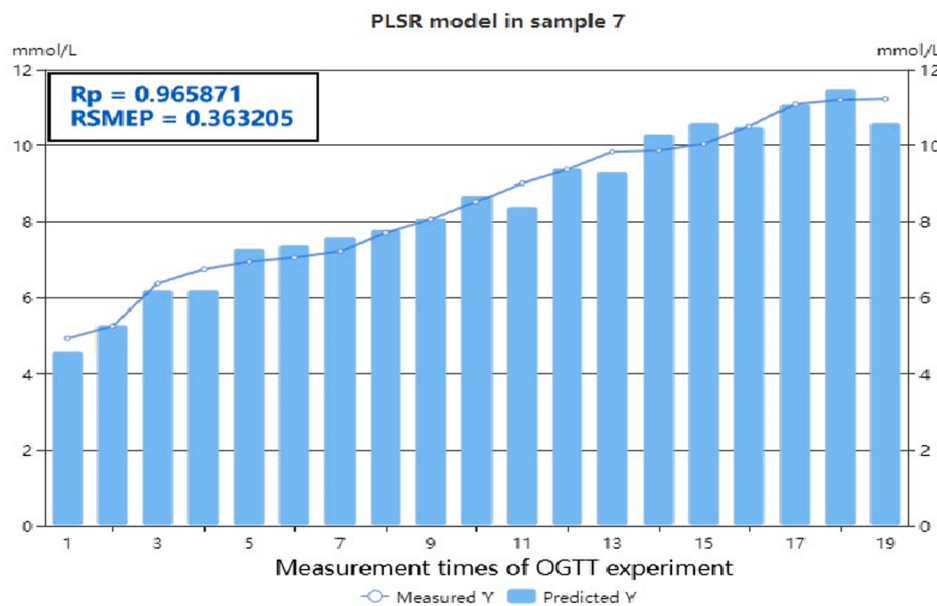


Fig. 7. Comparison of measured and predicted values of PLSR model in sample 7. Where column and line represented the measured and predicted values, respectively.

Table 3
Prediction result of PLSR and PLSR-SAE models.

Models	RMSEP (mmol/L)	R _p
PLSR (Average)	0.7212	0.7027
PLSR (OS 1)	1.6719	0.1670
PLSR (OS 2)	1.3929	0.3021
SAE (OS 1)	1.3368	0.8373
PLSR-SAE (OS 2)	1.0151	0.9216

points in region A, and have 31.96% and 2.04% sample points in region B, respectively. Accordingly, it demonstrates that the hybrid model of PLSR and SAE deep neural network is considerably better than the PLSR model when modeling multiple samples, which may be due to the fact that the SAE deep neural network can better suppress the influence of individual differences.

Moreover, we analyzed the EGA results predicted by SAE and PLSR-SAE models. As shown in Fig. 8(c) and (d), the proportion of sample points in regions A is 80.90% and 97.96%, whereas the proportion in region B is 19.10% and 2.04% in SAE and PLSR-SAE models respectively. The present findings have confirmed that the prediction accuracy of SAE model could be improved by using the PLSR screening process of multiple samples defined as an input.

4.2.2. Comparison between SVR and PLSR-SAE model

Furthermore, we use SVR model to model the OS 1 and compare the prediction accuracy. Comparing the measured and predicted blood glucose concentrations in SVR model for OS 1 and OS 2, the correlation coefficients (R_p) of 0.7302 and 0.8243, respectively, as shown in Fig. 9 (a) and (b). It demonstrates that the screening process of PLSR model does not significantly improve the prediction accuracy of SVR model. However, we compared the prediction results of SVR and PLSR-SAE models, the correlation coefficients (R_p) of 0.8243 and 0.9216, respectively. The results show that PLSR combined with SAE model can significantly improve the prediction accuracy of blood glucose concentration.

Therefore, it has been shown that the prediction accuracy of the noninvasive blood glucose predication method based on integrated PLSR model with SAE deep neural network meets the precision range of clinical laboratory standards, which has certain potential in clinical

research and trials.

5. Discussion

The present paper proposes a hybrid prediction method based on combination of linear and nonlinear regression models in order to improve the prediction accuracy and versatility of the noninvasive blood glucose predication method. A noninvasive blood glucose predication method was based on an integrated PLSR model with SAE deep neural network. During data modeling processes, the output of PLSR model was defined as an input of SAE model in order to improve a prediction accuracy of the final outcomes.

The present findings demonstrate that the prediction effect of PLSR model is superior to the PLSR-SAE model, when modeling a single sample. However, the PLSR-SAE model facilitates greater prediction accuracy than PLSR model when modeling multiple samples as a single input. Specifically, for example, the prediction results of multiple samples demonstrated that RMSEP values were 1.3929 mmol/L and 1.0151 mmol/L with a correlation coefficient of prediction of 0.3021 and 0.9216 in PLSR and PLSR-SAE models, respectively. Furthermore, in Clarke error grid analysis, the proportion of the points in regions A and B were 67.58% and 31.96% in PLSR model, respectively, whereas the PLSR-SAE model could achieve 97.96% of points in A region. When comparing SVR with PLSR-SAE models, the correlation coefficients (R_p) were 0.8243 and 0.9216, respectively.

However, the PLSR screening process cannot significantly improve the prediction effect in PLSR and SVR models of multiple samples, but it may improve the prediction accuracy in the SAE model. In addition, PLSR is a linear regression method based on Lambert Beer law, but in the near-infrared band, the relationship between the glucose absorption spectrum and its concentration is nonlinear for the strong scattering. Therefore, the SAE deep neural network may be more suitable for the noninvasive blood glucose predication of multiple samples by using a nonlinear regression approach.

Nevertheless, limitations are inevitable in any experimental work and should be discussed here for completeness. There is a considerable difference in dynamic physiological factors (e.g. human skin, tissue fluid, blood vessel distribution, blood pressure, body temperature) and in physiological state (e.g. the change of skin hydration with time) in each subject, which may cause the changes in optical parameters, and

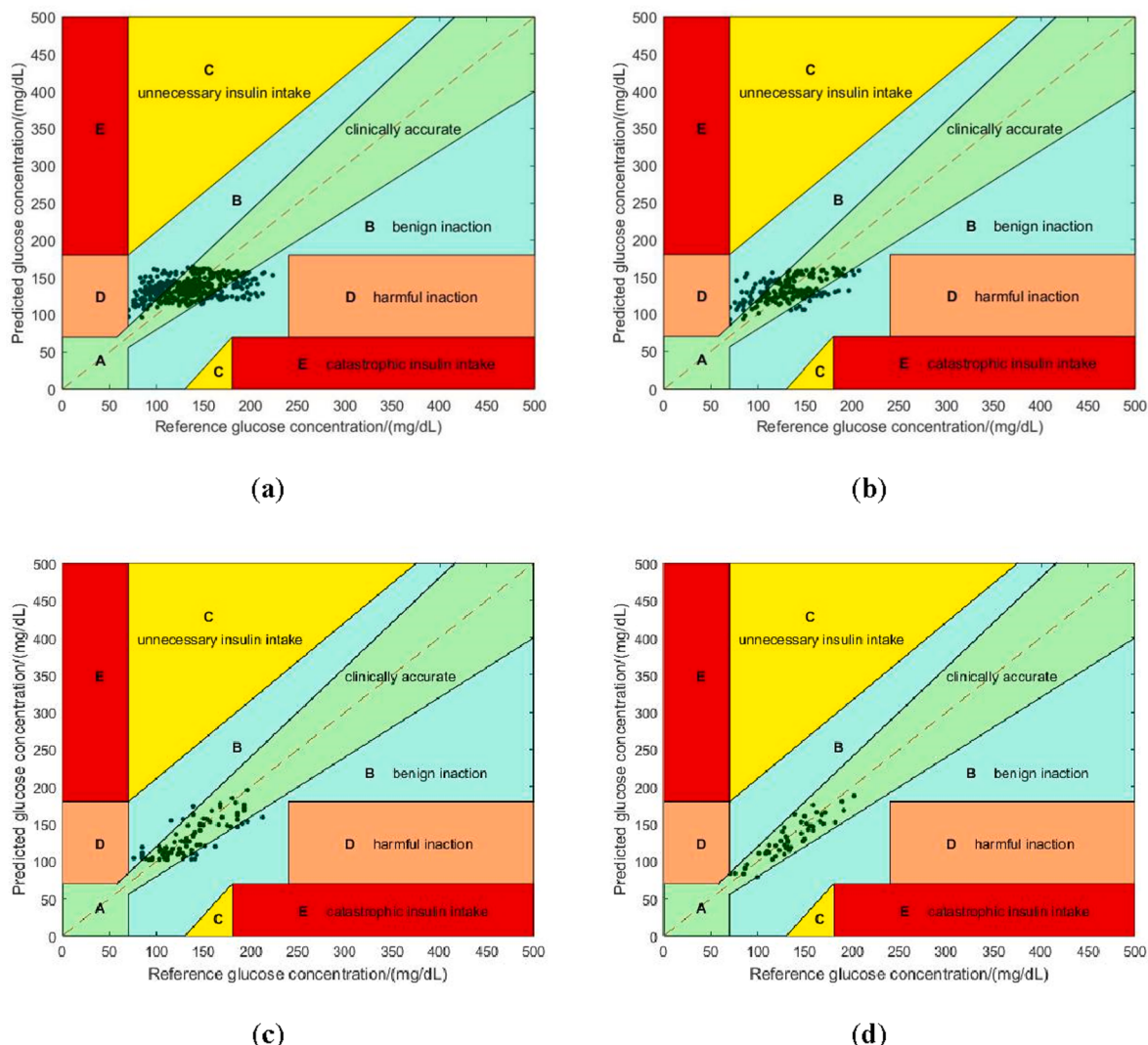


Fig. 8. Clarke EGA demonstrated the error grid analysis between the reference and measured values. The X and Y-axis represented the measured and predicted value of blood glucose concentration level, respectively. It divides the present plot into five different regions, the points in regions A and B are the most clinically relevant and acceptable points. (a) Clarke EGA of PLSR model in OS 1; (b) Clarke EGA of PLSR model in OS 2; (c) Clarke EGA of SAE model in OS 1; (d) Clarke EGA of PLSR-SAE model in OS 2.

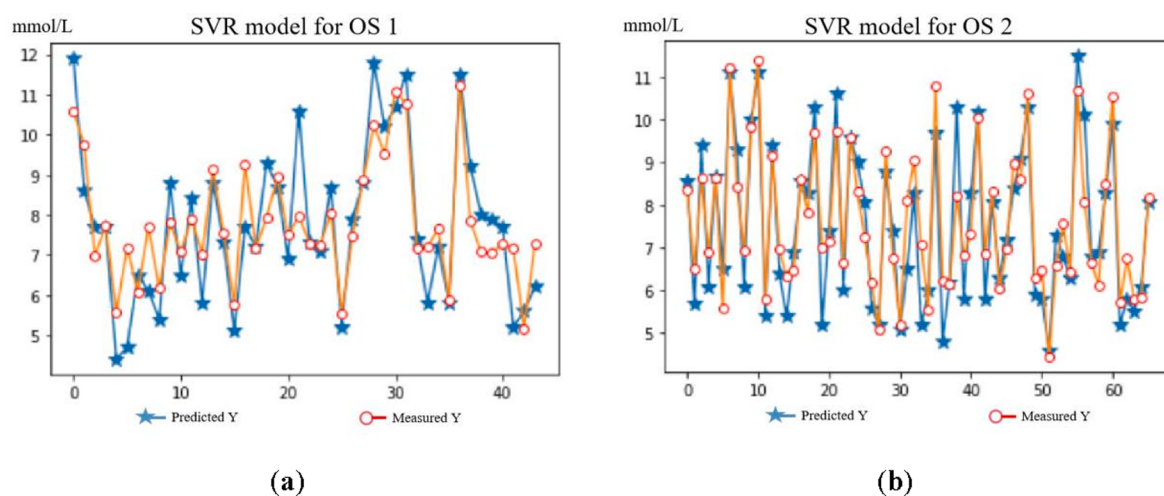


Fig. 9. Prediction results of SVR model. The star (blue) point and circular (red) point represented the predicted and measured value of blood glucose concentration level, respectively. (a)SVR model for OS 1; (b)SVR model for OS 2. (For interpretation of the references to colour in this figure legend, the reader is referred to the web version of this article.)

hence, interfere with the blood glucose measurements. Likewise, the error of experimental environmental factors (such as air pressure, humidity, temperature) and physical factors (such as light source drift, temperature and position change of measurement position) may have a certain effect on the accuracy of the spectral data. Therefore, when modeling multiple samples, the PLSR model facilitates worse prediction effects of multiple samples than in a single sample.

6. Conclusions

To conclude, the present study proposes, for the first time in the literature, a new solid modeling approach based on an integrated PLSR and SAE deep neural network to improve the prediction accuracy and versatility of noninvasive blood glucose predication methods. It has been demonstrated that the hybrid model of PLSR and SAE has better prediction accuracy than the PLSR model when modeling multiple samples. This may be due to the fact that the SAE deep neural network can better suppress the influence of individual differences, and optimize the limitations of the prediction system to multiple samples. Furthermore, PLSR-SAE model has better prediction effect than SVR method. Clarke error grid analysis shows that the prediction accuracy of the noninvasive blood glucose predication method based on this proposed model might meets the precision range of clinical laboratory standards, which has certain potential in clinical research and trials. Accordingly, this study demonstrated a potential of combining linear and nonlinear regression models in both, scientific and clinical research. A next relevant research step would be to determine the accuracy and feasibility of the PLSR-SAE model in large-scale experiments and across diverse data samples, Including people with diabetes. With that being said, in the future, there will be certainly safer and simpler methods for noninvasive blood glucose detection, which will result in as accurate detection method as invasive methods nowadays.

Funding

This work was funded by National Natural Science Foundation of China [61905176, 81901789], the Natural Science Foundation of Tianjin [20JCQNJC00150] and China Postdoctoral Science Foundation [2019M651036].

Declaration of Competing Interest

The authors declare that they have no known competing financial interests or personal relationships that could have appeared to influence the work reported in this paper.

Acknowledgments

The authors are grateful to all the volunteers for their cooperation in the experiments. Near-infrared spectroscopic measurement was conducted at the School of Precision Instruments and Optoelectronics Engineering, Tianjin University.

References

- [1] International Diabetes Federation. IDF Diabetes Atlas, 9th edn. Brussels, Belgium, 2019, Available online: <http://www.diabetesatlas.org>.
- [2] K. Maruo, M. Tsurugi, M. Tamura, Y. Ozaki, In vivo noninvasive measurement of blood glucose by near-infrared diffuse-reflectance spectroscopy, *Appl. Spectrosc.* 57 (2003) 1236–1244.
- [3] D.C. Klonoff, Continuous glucose monitoring: roadmap for 21st century diabetes therapy, *Diabetes Care* 28 (2005) 1231–1239.
- [4] O. Veiseh, B. Tang, K. Whitehead, Managing diabetes with nanomedicine: challenges and opportunities, *Nat. Rev. Drug Discov.* 14 (2015) 45–57.
- [5] M. Gusev, L. Poposka, G. Spasevski, Noninvasive glucose measurement using machine learning and neural network methods and correlation with heart rate variability, *J. Sens.* 2020 (2020) 1–13.
- [6] A. Tura, A. Maran, G. Pacini, Non-invasive glucose monitoring: assessment of technologies and devices according to quantitative criteria, *Diabetes Res. Clin. Pract.* 77 (2007) 16–40.
- [7] P.P. Pai, P.K. Sanki, S. Sarangi, S. Banerjee, Modelling, verification, and calibration of a photoacoustics based continuous non-invasive blood glucose monitoring system, *Rev. Sci. Instrum.* 86 (2015).
- [8] J.Z. Li, T. Igbe, Y.H. Liu, An approach for noninvasive blood glucose monitoring based on bioimpedance difference considering blood volume pulsation, *IEEE Access* 6 (2018) 51119–51129.
- [9] S.J. Yeh, C.F. Hanna, O.S. Khalil, Monitoring blood glucose changes in cutaneous tissue by temperature-modulated localized reflectance measurements, *Clin. Chem.* 49 (2003) 924–934.
- [10] C.E.F. Do Amaral, B. Wolf, Current development in non-invasive glucose monitoring, *Med. Eng. Phys.* 30 (2008) 541–549.
- [11] A. Ciudin, C. Hernandez, R. Simo, Non-invasive methods of glucose measurement: current status and future perspectives, *Curr. Diabetes Rev.* 8 (2012) 48–54.
- [12] R.A. Gabbay, S. Sivarajah, Optical coherence tomography-based continuous noninvasive glucose monitoring in patients with diabetes, *Diabetes Technol. Ther.* 10 (2008) 188–193.
- [13] Y.T. Lan, Y.P. Kuang, L.P. Zhou, Noninvasive monitoring of blood glucose concentration in diabetic patients with optical coherence tomography, *Laser Phys. Lett.* 14 (2017).
- [14] F. Foroughi, M. Rahsepar, M.J. Hadianfar, H. Kim, Microwave-assisted synthesis of graphene modified CuO nanoparticles for voltammetric enzyme-free sensing of glucose at biological pH values, *Microchim. Acta* 185 (2018).
- [15] J.X. Cheng, Z. Ji, M.Z. Li, Study of a noninvasive blood glucose detection model using the near-infrared light based on SA-NARX, *Biomed. Signal Process. Control* 56 (2020).
- [16] Z. Li, G. Li, W.J. Yan, L. Lin, Classification of diabetes and measurement of blood glucose concentration noninvasively using near infrared spectroscopy, *Infrared Phys. Technol.* 67 (2014) 574–582.
- [17] K. Maruo, T. Oota, M. Tsurugi, New methodology to obtain a calibration model for noninvasive near-infrared blood glucose monitoring, *Appl. Spectrosc.* 60 (2006) 441–449.
- [18] J. Yadav, A. Rani, V. Singh, B.M. Murari, Prospects and limitations of non-invasive blood glucose monitoring using near-infrared spectroscopy, *Biomed. Sig. Process. Control* 18 (2015) 214–227.
- [19] J. Kottmann, J.M. Rey, J. Luginbuehl, Glucose sensing in human epidermis using mid-infrared photoacoustic detection, *Biomed. Opt. Express* 3 (2012) 667–680.
- [20] R. Pandey, S.K. Paidi, T.A. Valdez, Noninvasive monitoring of blood glucose with Raman spectroscopy, *Acc. Chem. Res.* 50 (2017) 264–272.
- [21] N. Li, H. Zang, H.M. Sun, A noninvasive accurate measurement of blood glucose levels with Raman spectroscopy of blood in microvessels, *Molecules* 24 (2019).
- [22] H. Ali, F. Bensaali, F. Jaber, Novel approach to non-invasive blood glucose monitoring based on transmittance and refraction of visible laser light, *IEEE Access* 5 (2017) 9163–9174.
- [23] A. Aliberti, I. Pupillo, S. Terna, A multi-patient data-driven approach to blood glucose prediction, *IEEE Access* 7 (2019) 69311–69325.
- [24] L.W. Zhang, J. Lin, B. Liu, A review on deep learning applications in prognostics and health management, *IEEE Access* 7 (2019) 162415–162438.
- [25] X. Zhang, Y. Yang, Y.L. Wang, Q. Fan, Detection of the BRAF V600E mutation in colorectal cancer by NIR spectroscopy in conjunction with counter propagation artificial neural network, *Molecules* 24 (2019).
- [26] R.J. Chen, W.W. Wu, H.F. Qi, A Stacked autoencoder neural network algorithm for breast cancer diagnosis with magnetic detection electrical impedance tomography, *IEEE Access* 8 (2020) 5428–5437.
- [27] H.Q. Wang, W. Wu, Y. Cai, Optimization of reconstruction accuracy of anomaly position based on stacked auto-encoder neural networks, *IEEE Access* 7 (2019) 116578–116584.
- [28] Y.F. Chen, Y. Chen, X.P. Feng, Variety identification of orchids using fourier transform infrared spectroscopy combined with stacked sparse auto-encoder, *Molecules* 24 (2019).
- [29] B.S. Gurevich, S.Y. Dudnikov, V.V. Shapovalov, I.G. Zagorskii, Application of a spectroscopic method for noninvasive determination of glucose content in blood, *Russ. Phys. J.* 61 (2019) 2324–2326.
- [30] G. Han, F. Liu, Y. Tian, Detection of glucose concentration in a turbid medium using a stacked auto-encoder deep neural network, *Infrared Phys. Technol.* 105 (2020).
- [31] L. Vareka, P. Mautner, Stacked autoencoders for the P300 component detection, *Front. Neurosci.* 11 (2017).